J. Fluid Mech. (1990), *vol.* 220, *pp.* 339–354
Printed in Great Britain

The compressible vortex pair

By S. D. HEISTER†, J. M. McDONOUGH‡, A. R. KARAGOZIAN AND D. W. JENKINS

Mechanical, Aerospace and Nuclear Engineering Department, University of California, Los Angeles, CA 90024, USA

(Received 1 September 1988 and in revised form 13 April 1990)

A numerical solution for the flow field associated with a compressible pair of counter-rotating vortices is developed. The compressible, two-dimensional potential equation is solved utilizing the numerical method of Osher *et al.* (1985) for flow regions in which a non-zero density exists. Close to the vortex centres, vacuum 'cores' develop owing to the existence of a maximum achievable flow speed in a compressible flow field. A special treatment is required to represent these vacuum cores. Typical streamline patterns and core boundaries are obtained for upstream Mach numbers as high as 0.3, and the formation of weak shocks, predicted by Moore & Pullin (1987), is observed.

1. Introduction

Since Lord Kelvin's work, the incompressible vortex pair has represented a classic solution of the two-dimensional potential equation. Because this equation is linear, the superposition of two counter-rotating vortices located at the dimensional coordinates $\hat{y} = \pm h$, $\hat{x} = 0$ with a uniform crossflow yields a closed 'recirculation cell' which is approximately elliptic in shape. The resulting solution has application to flows over blunt elliptical bodies as well as jet and wake modelling efforts for effectively incompressible flows.

The development of high-speed aerospace vehicles in the twentieth century has produced interest in a similar type of representation for the compressible vortex pair. The problem has not been deemed tractable until very recently, with the advent of high-speed computers and a more thorough understanding of compressible fluid flow. The single compressible vortex has been studied over the years by Mack (1959), Brown (1965), and Ringleb (1940), and has been described by Shapiro (1953) and Kucheman (1978). Compressibility effects on a vortex ring have also been studied by Moore (1985), but direct application of these solutions to the compressible vortex pair is not straightforward. In 1987, Moore & Pullin made the first attempt to construct a solution to the compressible vortex pair itself, as will be discussed below.

Figure 1 highlights some of the physical differences between the compressible and incompressible vortex-pair recirculation cells. The incompressible cell enjoys a symmetry about both $\hat{x}$- and $\hat{y}$-axes, with intercepts at $\hat{x} = \pm\sqrt{3}h$, $\hat{y} \simeq \pm 2.09h$. The compressible cell is complicated by the presence of a vacuum core which surrounds each vortex centre, as well as the possibility of a shock existing in the recirculating region (for $\hat{x} > 0$). The vacuum core arises from the fact that there is a maximum achievable flow speed in a compressible fluid, at which vacuum conditions exist.

† Present address: School of Aeronautics and Astronautics, Purdue University, IN 47907, USA.
‡ Present address: Department of Mechanical Engineering, University of Kentucky, KY 40506, USA.

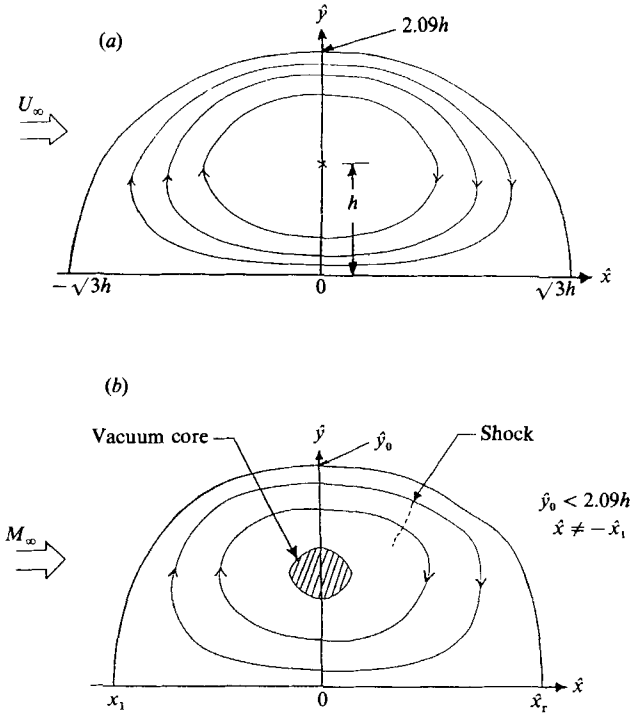

FIGURE 1. Comparison of features of (*a*) incompressible and (*b*) compressible vortex-pair recirculation cells.

Since for a compressible vortex one can show that qr = constant, where q is the flow speed and r the radial distance from the vortex centre, we must have a vacuum region surrounding any inviscid compressible vortex in an isentropic flow field.

In addition to the complication associated with a vacuum region, Moore & Pullin (1987), Manwell (1971), and others have noted the possibility of shocks existing in the recirculating region where $\hat{x} > 0$, owing to the deceleration of the flow from supersonic to subsonic speeds. This factor destroys the symmetry about the $\hat{y}$-axis in this flow, although symmetry about $\hat{y} = 0$ remains. Also note that compressibility affects the $\hat{x}$ and $\hat{y}$ intercept locations and that asymmetries due to the shock can cause the intercepts $\hat{x}_r$ and $\hat{x}_l$ to differ in figure 1.

In 1987, Moore & Pullin obtained a solution for the compressible vortex pair by employing the hodograph equations of transonic flow and mapping the resulting solution from the (q, θ) hodograph plane to the physical plane. Unfortunately, the mapping breaks down for a free-stream Mach number above 0.0875. The contribution of the present work is to provide a compressible vortex-pair solution for higher free-stream Mach numbers.

Because of the inability of the Moore & Pullin method to yield solutions at fairly low Mach number, a new approach is taken here which utilizes a numerical solution in the physical $(\hat{x}, \hat{y})$-plane. The solution technique relies on the assumption that, far from the vortex pair, the flow field may be characterized by superposition of a uniform stream and a Prandtl–Glauert dipole. The flow is assumed to be isentropic so that a velocity potential exists. The two-dimensional full potential equation is solved using the method of Osher, Hafez & Whitlow (1985) in the region where non-zero density

exists, and an exact solution is provided for the region within the vacuum cores. The Osher scheme allows for the presence of weak shocks, since the entropy jump across the shock is third order in the shock strength.

Section 2 discusses the equations governing flow in the fluid and vacuum regions, while §3 describes the discretization and solution of these equations. Results and conclusions are presented in §§4 and 5, respectively.

2. Governing equations in fluid and vacuum regions

As discussed previously, we consider a two-dimensional, compressible potential flow, and shocks, if present, must be weak in order not to violate the constant entropy condition. Referring to figure 1, we assume that as $\hat{x} \to -\infty$ we have flow parallel to the $\hat{x}$-axis, with conditions u_∞, M_∞, and ρ_∞ representing the velocity, Mach number, and density, respectively. Flow variables are non-dimensionalized with respect to these upstream conditions, while coordinates $\hat{x}$ and $\hat{y}$ are non-dimensionalized with respect to h, becoming x and y, respectively.

The governing equations are expressed in terms of the dimensionless velocity potential, ϕ, in order that only a single partial differential equation need be solved. We note, as above, that the full nonlinear, two-dimensional potential equation must be solved, since perturbation or small-disturbance theory cannot be applied to this truly two-dimensional flow in a neighbourhood of the vortex. Under these assumptions, the governing equation for ϕ (in conservative form) becomes

$$(\rho\phi_x)_x + (\rho\phi_y)_y = 0, \tag{1}$$

where ρ is the local gas density, and subscripts denote partial differentiation. The density can be related to the flow speed, q, and the free-stream Mach number, M_∞, using the isentropic relation:

$$\rho = [1 + \tfrac{1}{2}(\gamma-1)M_\infty^2(1-q^2)]^{1/\gamma-1} \tag{2}$$

where γ is the ratio of specific heats (assumed here to equal 1.4). The flow speed is calculated directly from the velocity potential:

$$q^2 = \phi_x^2 + \phi_y^2. \tag{3}$$

One can determine the maximum attainable flow speed, $q_{\max}$, by setting $\rho = 0$ in (2):

$$q_{\max}^2 = 1 + 2/((\gamma-1)M_\infty^2), \tag{4}$$

which demonstrates the fact that $q_{\max}$ decreases with increasing Mach number. For a single compressible vortex, Shapiro (1953) demonstrates that $qr = \Gamma/2\pi$, where Γ is the vortex circulation non-dimensionalized by hu_∞. Setting $q = q_{\max}$ in this relation allows one to calculate the dimensionless radius of the vacuum core for a single vortex, r_{vac},

$$r_{\text{vac}} = \frac{\Gamma}{2\pi}[1 + 2/((\gamma-1)M_\infty^2)]^{-\frac{1}{2}}, \tag{5}$$

indicating that r_{vac} increases with upstream Mach number M_∞. For this reason, the vacuum core will become more prominent as M_∞ is increased and will shrink to $r_{\text{vac}} = 0$ in the incompressible limit of $M_\infty = 0$. It will be useful here to substitute (4) into (5) to obtain

$$r_{\text{vac}} = \frac{\Gamma}{2\pi q_{\max}}. \tag{6}$$

Labelling the sonic condition as ( )* we can show that

$$q^* = ((2/M_\infty^2 + \gamma - 1)/(\gamma + 1))^{\frac{1}{2}} \tag{7}$$

and $\rho^* = \rho(q^*)$, as defined in (2). Therefore, when $q > q^*$ we have supersonic flow, and when $q < q^*$ the flow is subsonic.

As mentioned above, we make use of the Prandtl–Glauert transformation applied to a vortex-pair dipole in order to obtain a solution for ϕ far from the cell boundary. Based on this straightforward transformation, the expression for the compressible, non-dimensional velocity potential in the far field becomes

$$\phi_{\rm ff} = \frac{\Gamma}{\pi(1-M_\infty^2)^{\frac{1}{2}}}\left[\tfrac{1}{4}x + \frac{x}{(x^2 + (1-M_\infty^2)\,y^2)}\right]. \tag{8}$$

For the far-field result to be complete we require a value for the dimensionless circulation, Γ. For the classical incompressible vortex pair, it can be shown that $\Gamma = 4\pi$. Moore & Pullin (1987) derive a correction to this result in the compressible case, assuming small vacuum cores:

$$\Gamma = 4\pi/(1-\tfrac{1}{4}M_\infty^2). \tag{9}$$

This expression for dimensionless circulation is used by these researchers when the result for $\phi_{\rm ff}$ is required. Although the relation holds only for small cores, we shall apply it for the case of higher Mach numbers (and hence larger cores) as an initial guess in an iteration process since the correction is small, even for higher values of M_∞. Results will prove to be insensitive to the circulation far from the cell, where the result applies in any case. Finally, we note that (8) provides excellent initial values for ϕ when used as an input to the overall iterative solution method (see §3).

The equation governing ϕ within the vacuum regions is not as easily defined; we are not aware of any prior formulations of such a relation. Vacuum regions have been simulated in some blast wave calculations, but they arise only in numerical schemes owing to the large drop in pressure across the wave. To gain some insight, consider the non-conservative form of the velocity potential equation as derived in Anderson (1982), for example:

$$(1-(\phi_x/c)^2)\,\phi_{xx} + (1-(\phi_y/c)^2)\,\phi_{yy} - 2\phi_x\phi_y\phi_{xy}/c^2 = 0, \tag{10}$$

where $c^2 = \gamma p/\rho$ represents the square of the sound speed in the fluid. Now since the flow is isentropic, $p \sim \rho^\gamma$, so that c must vanish as ρ vanishes in the vacuum region. Under this limit ($c \to 0$) the potential equation (10) becomes

$$\phi_x^2\phi_{xx} + \phi_y^2\phi_{yy} + 2\phi_x\phi_y\phi_{xy} = 0, \tag{11}$$

which is actually nonlinearly degenerate. In vector notation, (11) reduces to

$$\bar{V}\cdot\bar{\nabla}(\tfrac{1}{2}q^2) = 0,$$

which appears to provide no additional information (consistent with the degeneracy) since $q = q_{\max} = $ const. in the vacuum core. But simply from the definition of q we have

$$\phi_x^2 + \phi_y^2 = q_{\max}^2, \tag{12}$$

which is recognized as the eikonal equation of geometric optics. Exact solutions to this equation are easily obtained; hence ϕ within the core can, in principle, be found exactly.

As a final note in the flow-field description, we derive the relation between the compressible stream function and the velocity potential. The compressible stream function is defined:

$$\psi_y = (\rho/\rho_0)\,\phi_x, \tag{13}$$

$$\psi_x = -(\rho/\rho_0)\,\phi_y, \tag{14}$$

where ρ_0 corresponds to the stagnation density. Integrating (13) with respect to y and (14) with respect to x, and requiring $\psi = 0$ on the symmetry plane, leads to the following expression for the stream function in terms of the velocity potential:

$$\psi(x,y) = \int_0^y \frac{\rho}{\rho_0}\phi_x\,\mathrm{d}y - \int_0^x \frac{\rho}{\rho_0}\phi_y\,\mathrm{d}x + \left[\int_0^y \frac{\rho}{\rho_0}\phi_x\,\mathrm{d}y\right]_{x=0}, \tag{15}$$

where the arbitrary factor of 0.5 has been omitted. This equation can be used to determine streamlines once ϕ and ρ are known throughout the grid.

3. Analysis and discretization of governing equations

From the foregoing discussion we can now formulate the complete mathematical problem needed to describe the flow field associated with the compressible vortex pair. As already noted, the flow is symmetric with respect to the x-axis, so the formal mathematical description is given as the solution to (1) in the half-plane above the x-axis (external to the vacuum core) and the solution to (12) within the vacuum core. The precise boundary conditions for (1) are

$$\phi_x \to \frac{\Gamma}{4\pi(1-M_\infty^2)^{\frac{1}{2}}} \quad \text{as} \quad |x| \to \infty, \tag{16a}$$

$$\phi_y \to 0 \quad \text{as} \quad y \to \infty, \tag{16b}$$

$$\phi_y(x,0) = 0 \quad \text{for all } x, \tag{16c}$$

$$\phi(x,y) = \phi_c(x,y) \quad \text{on the vacuum core boundary}, \tag{16d}$$

where ϕ_c, the value of the dimensionless velocity potential at the vacuum core boundary, is thus far unknown. The first two conditions, (16*a*) and (16*b*), are consistent with the far-field condition (8). The last of these conditions, (16*d*), can also be viewed as the boundary condition for (12); that is, we require continuity of ϕ at the core boundary. We shall see below that this condition cannot be met exactly.

There are several important aspects of this problem that merit discussion prior to attempting a numerical solution. First, it follows from (2) and (3) that ρ in (1) is a function of ϕ, γ, and M_∞, thus it does not actually represent a separate variable. On the other hand, the presence of ρ in (1) results in a significant nonlinearity. Similarly, $q_{\max}$ in (12) is obtained from (4) as a function of γ and M_∞ only. The most significant point regarding the overall problem is that the vacuum core boundary is not known *a priori* and must be found as part of the solution. In addition, from (6) we see that the dimensionless circulation Γ will be involved in specifying the size of the core region. Γ itself is not known, however, except for very small values of M_∞ for which the core is small and (9) is valid. These features all influence the nature of the solution algorithm, and in particular lead to some modification of the boundary conditions employed for (1), as discussed in the following subsection.

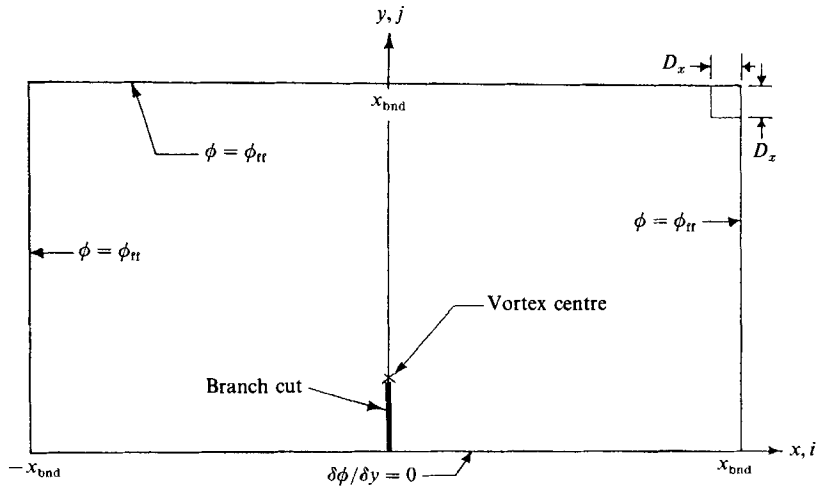

FIGURE 2. Computational domain for numerical calculation.

3.1. *The fluid region*

In the fluid region, external to the vacuum core, the governing equation, (1), is elliptic far from the core, but in a neighbourhood of the core it changes type to hyperbolic as the flow becomes supersonic. This implies that special care will be required in discretizing this equation. On the other hand, sufficiently far from the core the flow is uniformly subsonic (and, in fact, nearly incompressible) and is governed by the small-disturbance form of the potential equation. The exact solution to this equation far from the vortices is given in (8), and the availability of such a solution permits us to solve (1) on a finite domain, say $(-x_{bnd}, x_{bnd}) \times [0, y_{bnd})$, and to use (8) to provide Dirichlet conditions on all boundaries except the symmetry plane. The main restriction on this approach is that x_{bnd} and y_{bnd} must be sufficiently large that the assumptions of small-disturbance theory are valid. It is important to note, however, that the formula to be used for evaluating the Dirichlet conditions contains the unknown circulation, Γ. The complete formulation of the boundary conditions associated with the finite fluid region thus replaces conditions (16*a*, *b*) with

$$\phi(x, y) = \phi_{ff}(x, y) \tag{17}$$

at the outer boundaries of the computational domain. The problem is presented schematically in figure 2, in which we take $y_{bnd} = x_{bnd}$. The presence of a branch cut is noted since this also must be properly taken into account in any numerical treatment.

We shall present the solution procedure for the fluid region problem under the assumption that Γ, ϕ_c, and the core boundary are known. We develop an exact expression for ϕ_c and an associated prescription for the core boundary in the next subsection. It is interesting to note that essentially all of the aspects of this fluid region problem are present in a very different problem treated by Shankar *et al.* (1987), and our approach closely parallels theirs. In particular, under the assumptions that we have made thus far, the two most difficult parts of the computational problem are the transformation to generalized coordinates, and the treatment of type changes in (1), including weak shocks in its solution. The first of these is needed to provide an accurate solution of the core boundary and implementation of any

appropriate boundary conditions thereon; we have already noted the implications of the second of these.

Equation (1) can be written in generalized coordinates as

$$\left(\frac{\rho}{J}\Phi_\xi\right)_\xi+\left(\frac{\rho}{J}\Phi_\eta\right)_\eta=0, \tag{18}$$

where Φ_ξ and Φ_η are the contravariant velocity components in the generalized coordinate directions, ξ and η, and are defined as

$$\Phi_\xi \equiv (x_\eta^2+y_\eta^2)\,\phi_\xi+(x_\xi y_\xi+x_\eta y_\eta)\,\phi_\eta,$$

$$\Phi_\eta \equiv (x_\xi y_\xi+x_\eta y_\eta)\,\phi_\xi+(x_\xi^2+y_\xi^2)\,\phi_\eta.$$

In these expressions,

$$J \equiv x_\xi y_\eta - x_\eta y_\xi$$

is the Jacobian of the inverse transformation (from computational to physical coordinates), T^{-1}: $(\xi,\eta)\to(x,y)$, and ϕ_ξ and ϕ_η are obtained from ϕ_x and ϕ_y via the chain rule. Construction of T^{-1} is carried out numerically via transfinite interpolation (see Thompson, Warzi & Mastin 1985) and maps $(\xi,\eta)\in[-1,1]\times[0,2]$ to $(x,y)\in[-x_{\mathrm{bnd}},x_{\mathrm{bnd}}]\times[0,x_{\mathrm{bnd}}]$, such that $[-\frac{1}{2},\frac{1}{2}]\times[\frac{1}{2},\frac{3}{2}]$ maps to the core boundary. Hence, the transformation is a boundary-fitted coordinate system, fitted to the boundary of the vacuum core.

The discretization of (18) is done analogously to the approach taken in Shankar *et al.* (1987), the main difference here being that we seek steady solutions and hence employ a pseudo-transient representation, rather than the time-accurate approach of Shankar *et al.* Thus, we write (18) as

$$\phi_\tau-\left(\frac{\rho}{J}\Phi_\xi\right)_\xi-\left(\frac{\rho}{J}\Phi_\eta\right)_\eta=0 \tag{19}$$

and construct a backward Euler temporal discretization,

$$\phi^{n+1}=\phi^n+k\left[\left(\frac{\rho}{J}\Phi_\xi\right)_\xi+\left(\frac{\rho}{J}\Phi_\eta\right)_\eta\right]^{n+1}, \tag{20}$$

where k is the pseudo-time step, $k\equiv\Delta\tau$, and the superscripts denote pseudo-time indices, or equivalently, iteration counters. Because ρ is a function of ϕ, iterations are often useful within a pseudo-time step. At each such iteration we linearize (20) by evaluating ρ with the previous iterate of ϕ, and write the result as

$$\left\{I-k\left[\frac{\partial}{\partial\xi}\left(\rho^0\frac{\partial}{\partial\xi}\right)+\frac{\partial}{\partial\eta}\left(\rho^0\frac{\partial}{\partial\eta}\right)\right]\right\}\delta\phi=\phi^0-\phi^n+k\left[\left(\frac{\rho}{J}\Phi_\xi\right)_\xi^0+\left(\frac{\rho}{J}\Phi_\eta\right)_\eta^0\right]. \tag{21}$$

In this expression, I is the identity matrix, 0 denotes evaluation at the previous iteration, and $\delta\phi\equiv\phi^{n+1}-\phi^0$. We note that when $\phi^0\to\phi^{n+1}$ the right-hand side of (21) is precisely (20), and thus is equal to zero. It follows that (21) is in the form of a Newton iteration with the term in brackets on the left-hand side being the Jacobian matrix of the function on the right-hand side, whose zero is to be found. It is because of the form of (21) that we have been able to neglect metric information arising from generalized coordinates on the left-hand side. In particular, it is well known that Newton iterations are convergent (at least locally) even when the exact Jacobian

matrix is not used. Thus, simple, convenient, and stable spatial discretizations can be employed on the left-hand side of (21), and more sophisticated and accurate methods will be applied on the right-hand side. We shall, however, retain conservation form on both sides of the equation.

In the discrete approximation of (21), first-order upwind differencing is employed on the left-hand side to adequately handle the type change (and hence qualitative solution properties with respect to wave propagation) of (1). Switching from upwind to downwind differencing is based on the contravariant velocity components, Φ_ξ and Φ_η, rather than on ϕ_x and ϕ_y. This generalized coordinate metric information is found to be necessary in order to guarantee unconditional stability of the pseudo-time marching.

The discrete form of the right-hand side of (21) is obtained using the Osher flux biasing procedure (see Osher *et al.* 1985), but in generalized coordinates as done by Shankar *et al.* (1987). The advantage of this scheme is its ability to automatically handle type changes in the potential equation, and sharply resolve weak shocks, while maintaining formal second-order accuracy away from shocks. Details of this method are provided in the Appendix.

The only remaining detail in the treatment of the fluid region is the approximation at the branch cut. Along $x = 0$, the solution for an incompressible vortex pair in a uniform stream produces the following dimensionless velocity potential at $x = 0$:

$$\phi_{\text{inc}}(0, y) = \begin{cases} 0 & (y > 1) \\ \pm\frac{1}{4}\Gamma & (y = 1) \\ \pm\frac{1}{2}\Gamma & (y < 1). \end{cases}$$

Here the plus sign corresponds to the right half-plane, and the minus sign is for the left half-plane, with the difference in sign due to the branch cut existing for $y \leqslant 1$. This incompressible solution is used as a first approximation to the velocity potential in this region. The computational procedure then updates ϕ-values along the branch cut as if the approach to this location were from the right half-plane. The ϕ-values required on the left-hand side of the branch cut are obtained by linear extrapolation from values adjacent to $x = 0$ on the right-hand side. Then, to ensure continuity in y-components of velocity along the branch cut, ϕ-values approaching from the left are taken to be the negative of those approaching from the right. Of course, this procedure is applied only to that segment of the branch cut lying outside the vacuum core.

3.2. *The vacuum core*

As already noted, the equation for ϕ inside the vacuum core is the eikonal equation. Exact solution can be found from the method of characteristics (see Garabedian 1964), but here we shall make use of a rather simple form of the solution that can be obtained by inspection. In particular, it is clear that (12) is satisfied by any function ϕ of the form

$$\phi(x, y) = ux + v(y - 1) + C, \tag{22}$$

where u, v and C are constants, and

$$v = (q_{\max}^2 - u^2)^{\frac{1}{2}}.$$

Moreover, because we expect the velocity in the core to be related to that in the fluid near the core, it appears that $u = \phi_x$. It is at this point that we recognize a basic deficiency with (22): namely, that ϕ_x changes sign across the line $y = 1$, and ϕ_y

changes sign across $x = 0$. Thus, the constants u and v in (22) can only be constant in magnitude, and we must view (22) as a weak solution to (12) with jump discontinuities due to required changes at $x = 0$ and $y = 1$. There are four separate pieces to this solution, and there are correspondingly four additional arbitrary constants, C_1, C_2, C_3, and C_4.

We next observe that merely setting u equal to ϕ_x does little to solve our complete problem because ϕ_x must be obtained from the numerical solution to the problem in the fluid region, and this will require data from the core. It can be shown that u is related to the core geometry and the circulation, Γ, in a specific way. In particular, if we circumscribe the core with a rectangle of sides D_x and D_y and evaluate the circulation, we obtain

$$\Gamma \approx 2[uD_x + (q_{\max}^2 - u^2)^{\frac{1}{2}} D_y]. \tag{23}$$

This result is not exact because we have taken u and v to be constant in magnitude around the path of integration, and part of this path lies off the core boundary where the velocity components differ somewhat from those in the core. It will be apparent from numerical results presented in §4 that the result of this discrepancy is small. Thus, we can solve (23) for u as if equality holds, and obtain

$$u = \frac{D_x \Gamma \pm D_y [4q_{\max}^2 (D_x^2 + D_y^2) - \Gamma^2]^{\frac{1}{2}}}{2(D_x^2 + D_y^2)}.$$

Hence u is determined uniquely if and only if

$$D_x^2 + D_y^2 = \frac{\Gamma^2}{4q_{\max}^2}. \tag{24}$$

This constraint provides a bound on the size of the vacuum core because D_x and D_y are, by definition, the extent of the core in the x- and y-directions, respectively. The similarity of (24) to (6) should be noted. In particular, if we take $D_x = D_y = 2r_{\text{vac}}$ we have

$$r_{\text{vac}} = \frac{\Gamma}{4\sqrt{2}q_{\max}},$$

which differs from the incompressible case by approximately 10%. It also follows from (24) that

$$u = \frac{2q_{\max}^2 D_x}{\Gamma}. \tag{25}$$

Equation (25), in conjunction with (22) and the proper choice of signs on u and v, determines ϕ_c within the vacuum core up to a constant to be set in each of the four regions.

The four constants are chosen to make ϕ as nearly continuous as possible when passing from the fluid region to the vacuum core. This is accomplished by linearly extrapolating fluid region values of ϕ to the core boundary at four different points around the core, corresponding to the four corners of the core in the computational domain, and choosing values of C_m ($m = 1, \ldots, 4$) to match these extrapolated values. Hence, ϕ_c is now completely determined within the core. It is also noteworthy that ϕ_c is not continuous around the boundary of the core, although this turns out to be of little importance because ϕ_c is used only at discrete points by the solution procedure for the fluid region.

The remaining task associated with analysis of the core region is determination of the core boundary. A boundary-fixed coordinate system is employed in the present study, and in order to generate the generalized coordinates of this system, the nature of the core shape must be prescribed. To accomplish this we employ two assumptions to complement the information contained in (24). The first of these arises from a careful examination of the vacuum core boundaries predicted by Moore & Pullin (1987). It is found that in general the radius of the predicted vacuum core is essentially the same as would be calculated from (6) for the incompressible case, that is, $D_x = D_y = 2r_{\text{vac}}$. Moreover, our own calculations confirm what Moore & Pullin assumed regarding symmetry of the core with respect to the y-axis, that is, $D_x = D_{x,\text{L}} + D_{x,\text{R}}$, with $D_{x,\text{L}} = D_{x,\text{R}}$. Here L and R subscripts denote left and right sides of the core, respectively. In addition, if we set $D_y = D_{y,\text{T}} + D_{y,\text{B}}$, with T and B denoting top and bottom, we find that $D_{y,\text{T}} < D_{y,\text{B}}$, again consistent with the observation of Moore & Pullin (1987). These observations, along with (24), the requirement for a unique determination of core velocity, suggest that a reasonable representation of the core boundary might be a generalized ellipse with semi-axes $D_{x,\text{L}}$, $D_{x,\text{R}}$, $D_{y,\text{T}}$ and $D_{y,\text{B}}$, so that the problem of specifying the core can be reduced to finding these four quantities.

Our preceding remarks suggest that $D_x = D_y$ should hold to a good approximation, hence this is used for an initial guess, but it is not required in subsequent iterations. In addition, if we define $\bar{q}_{\text{T}}$ to be the average flow speed in the fluid at the top of the core, and analogously $\bar{q}_{\text{B}}$ for the bottom, it is reasonable to assume that $D_{y,\text{T}} \sim 1/\bar{q}_{\text{T}}$ and $D_{y,\text{B}} \sim 1/\bar{q}_{\text{B}}$ for a vortical flow field. We then obtain

$$D_{y,\text{B}} = \frac{D_x}{1 + (\bar{q}_{\text{B}}/\bar{q}_{\text{T}})} \tag{26}$$

and

$$D_{y,\text{T}} = D_y - D_{y,\text{B}}. \tag{27}$$

$D_{x,\text{L}}$ and $D_{x,\text{R}}$ are found in a manner similar to that employed by Heister (1988), except that the test $q \leqslant q_{\max}$ is carried out only along the horizontal axis of the vacuum core, i.e. along the line $y = 1$. As mentioned earlier, we always find that $D_{x,\text{L}} = D_{x,\text{R}}$, although our procedure does not require this. We then have $D_x = D_{x,\text{L}} + D_{x,\text{R}}$ for use in (26), which is the same value used for D_y in (27).

Finally, we note that since the values of D_x and D_y are obtained as a by-product of the computed velocity potential ϕ from a previous estimate of the core geometry, the values may not satisfy the geometric constraint, (24), needed to guarantee a unique solution to (12). This occurs in the first step of the calculation because the initial core geometry is based on the solution to the small-disturbance equation rather than on the solution to the full potential equation, and it can occur in later steps because the circulation, Γ, may change from one pseudo-time step to the next. To remedy the situation, then, solution for a value α must be found, where

$$(\alpha D_x)^2 + (\alpha D_y)^2 = \frac{\Gamma^2}{4q_{\max}^2},$$

yielding

$$\alpha = \left[\frac{\Gamma^2/4q_{\max}^2}{D_x^2 + D_y^2}\right]^{\frac{1}{2}}. \tag{28}$$

The generalized ellipse semiaxes are then rescaled by the value of α.

3.3. *Solution algorithm*

In the preceding subsections the treatment of the fluid and vacuum core regions of the compressible vortex-pair flow field is discussed under the assumption that the circulation is known. Γ is required for setting the far-field boundary conditions in the fluid region computations, and it appears explicitly in formulae associated with the size of the vacuum core. For very small M_∞ an accurate approximation is provided by (9), but for larger M_∞, say $M_\infty \geqslant 0.1$, this may not be accurate. Thus, the overall computational procedure requires determination of Γ as part of the solution. Because the flow is assumed inviscid and approximately isentropic, Γ will be the same for any closed loop encircling the vacuum core, so if the correct value of Γ has been chosen to prescribe the far-field boundary conditions, we should obtain the same value by integrating the velocity field around an arbitrary path enclosing the vortex core. This velocity field also depends on M_∞, through $q_{\max}$ and the vortex core properties, so that the prescribed and calculated values of Γ will not coincide if the prescribed value is not consistent with the value of M_∞.

It is easy to show that an integration of the velocity field over a path one grid point away from the core boundary in the computational domain results in the expression

$$\Gamma = \phi_{i_{\mathrm{cc}}, j_{\mathrm{c}}-1} - \phi_{i_{\mathrm{bc}}, j_{\mathrm{c}}-1}, \tag{29}$$

where i_{cc} is the ξ-index of the core centre, j_{c} is the starting index of the core in the η-direction, and bc refers to a branch-cut value. But, as already noted, the calculated values of ϕ depend on Γ. Thus, (29) provides a fixed-point iteration for Γ:

$$\Gamma^{n+1} = G(\Gamma^n),$$

where G is the right-hand side of (29). This provides the final expression needed to compute a solution to the complete problem posed at the beginning of this section.

4. Results

As mentioned above, treatment of the vacuum region has not previously been attempted, and for this reason it is desirable to examine the core boundary shape predicted by the code. A rationale has been developed whereby the viability of the vacuum region computational approach is assessed by comparing core boundary results with Moore & Pullin's (1987) predictions. Because Moore & Pullin are only able to obtain results up to $M_\infty = 0.0875$, our predictive tests are limited to this value. A small discretization step size ($\Delta x = 0.0125$) is required in order to resolve the small core associated with this free-stream Mach number. Typical run times are approximately one minute on an IBM 3090-600S for the 161×161 grid required in this case.

The vacuum-region solution described in the previous section provides a good comparison with Moore & Pullin's results, as shown in figure 3. At free-stream Mach numbers above 0.04, the numerical solution tends to slightly overpredict the height of the vacuum core boundary above $y = 1$. If the solution by Moore & Pullin is considered to be the correct core shape, then this discrepancy is to be expected, since the upper portion of the core boundary is approximated by two generalized quarter-ellipses. The rest of the core boundary is represented quite accurately by the present calculation, however, and we find that the slight discrepancy at the top of the core for higher Mach numbers has a negligible effect on the prediction of the fluid region. Higher-Mach-number cases are thus run with reasonable confidence in their accuracy.

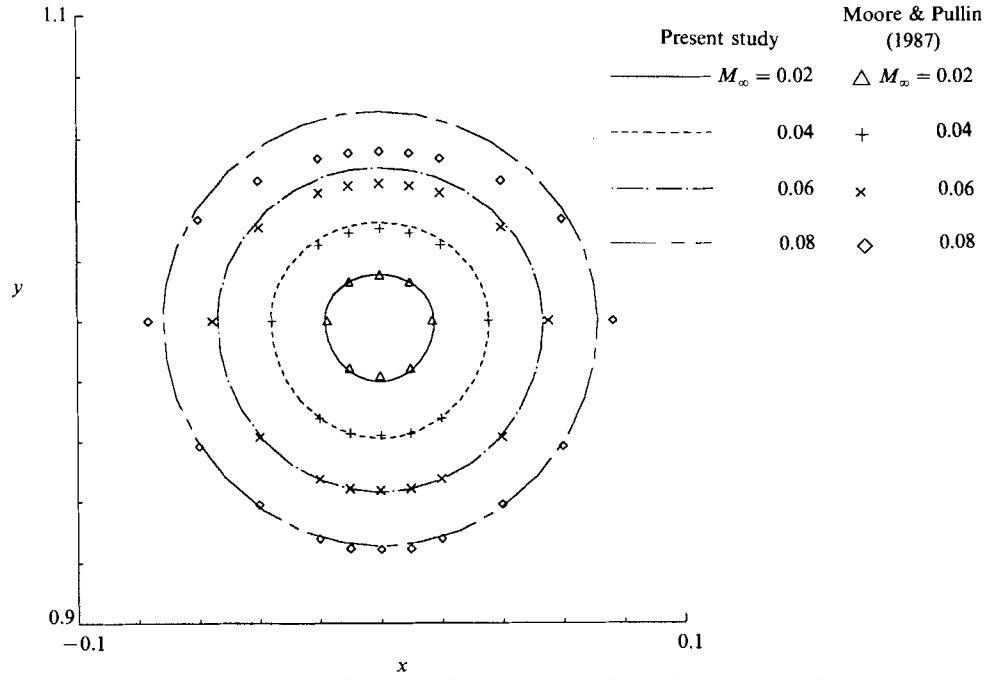

FIGURE 3. Comparison of computed vacuum core boundary with results of Moore & Pullin (1987).

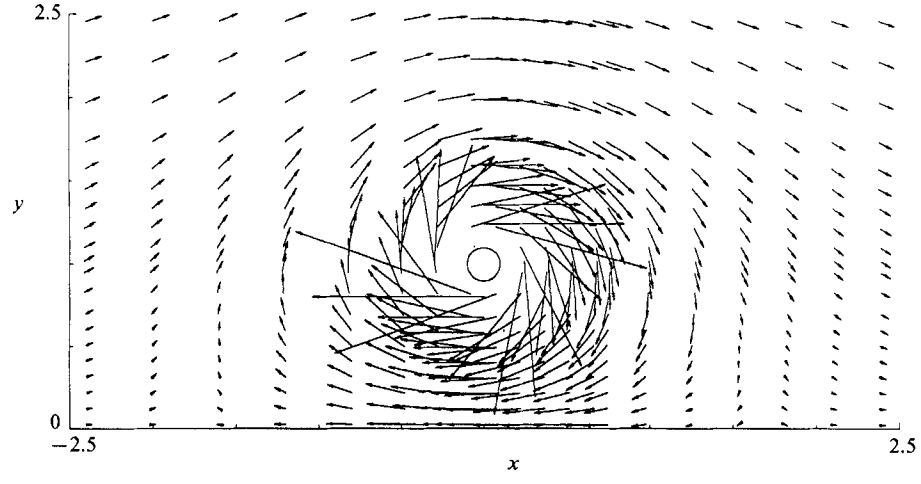

FIGURE 4. Vacuum core boundary and velocity vectors for $M_\infty = 0.1$.

Results for the flow field external to the vacuum core are presented in figures 4–7. Figures 4 and 5 present velocity vector plots and streamline patterns, respectively, calculated for $M_\infty = 0.1$, while figures 6 and 7 present results for $M_\infty = 0.3$. Some smoothing is required above the vacuum core along $x = 0$ owing to the presence of the branch cut. In figure 5 we see that the streamline patterns are nearly symmetric about the y-axis, as in the case of the incompressible vortex pair, while in figure 7, slight asymmetries are seen to develop, which increase in magnitude with M_∞. These

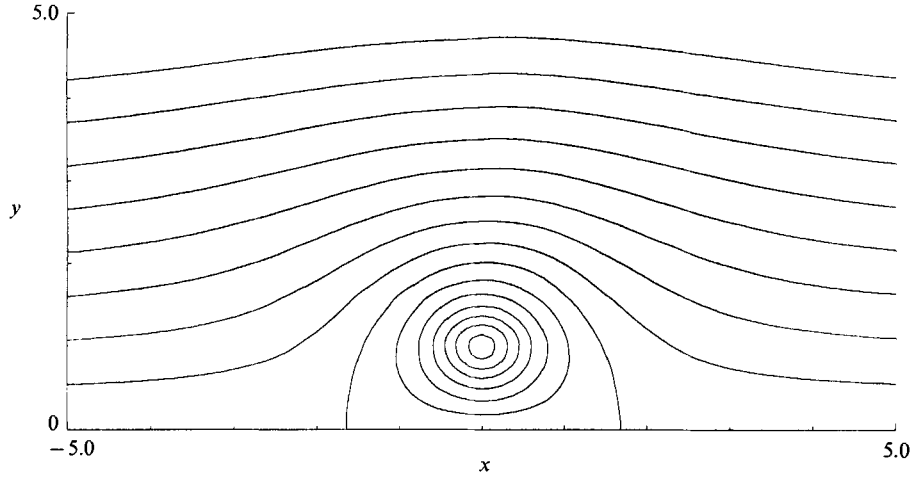

FIGURE 5. Streamline pattern for $M_\infty = 0.1$

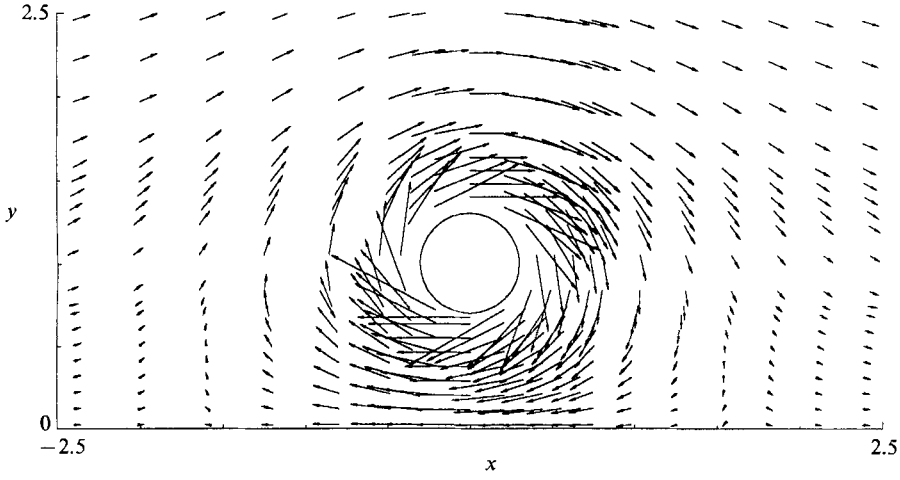

FIGURE 6. Vacuum core boundary and velocity vectors for $M_\infty = 0.3$.

are believed to be associated with a weak shock to the right of $x = 0$, as noted in figure 1. Results cannot be achieved easily above $M_\infty = 0.3$ because the vacuum core (and its associated errors) has grown to be a dominant feature of the cell and actually can exceed the recirculation cell boundaries.

Another interesting feature of the $M_\infty = 0.3$ results is a weak shock which appears in the recirculating region, as predicted by Moore & Pullin (1987) and Manwell (1971). The approximate shock location is noted in the schematic diagram in figure 1. The actual shock strength is greatest in the centre and vanishes as one traverses the shock lines to either end.

The growth in vacuum core size is demonstrated in figure 8, which presents core boundary shapes for $M_\infty = 0.1$, 0.2, 0.3, and 0.4. The core tends to be elongated slightly toward the origin. While inaccuracies in the model are such that results for $M_\infty = 0.4$ and above are very approximate, core size predictions are fairly insensitive to the approximation for Γ and to vacuum-region representation, and for this reason the $M_\infty = 0.4$ result is presented.

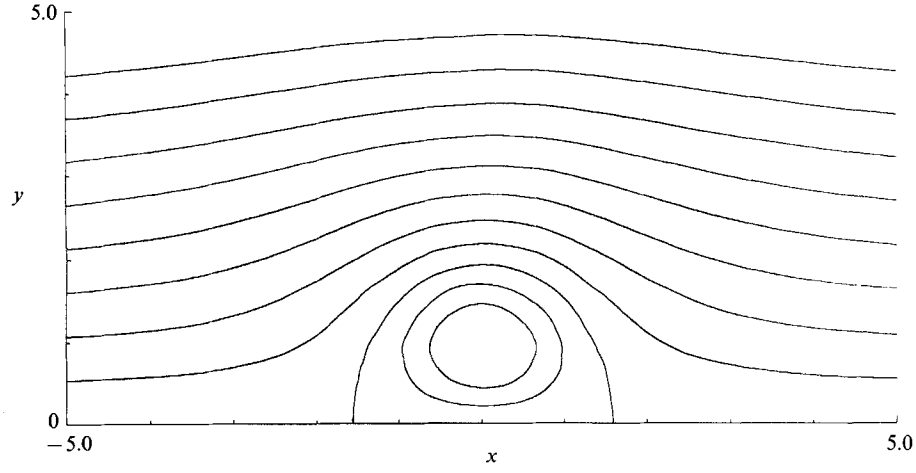

FIGURE 7. Streamline pattern for $M_\infty = 0.3$.

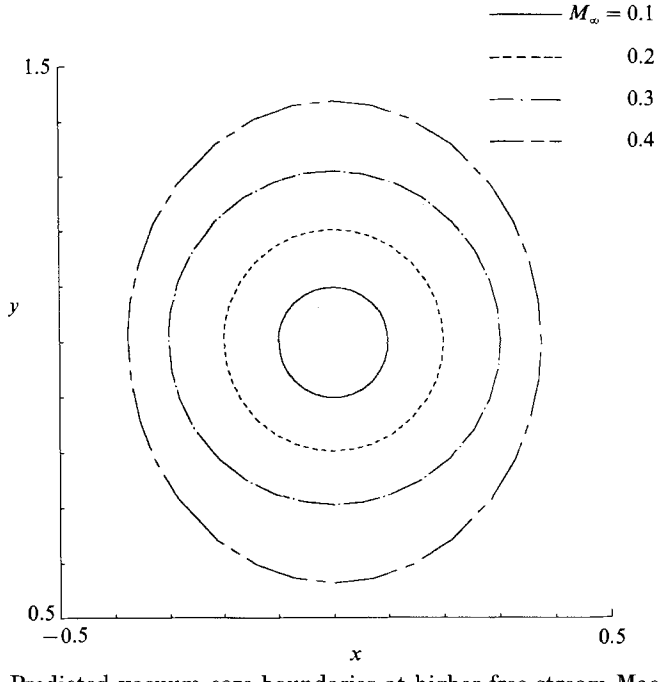

FIGURE 8. Predicted vacuum core boundaries at higher free-stream Mach numbers.

5. Conclusions

The solutions presented in this paper cannot be considered to be the final word on the compressible vortex pair, but instead should be viewed as a step toward gaining a better understanding of this complex and most interesting flow field. In a sense, we have used numerical means to extend the significant contributions of Moore & Pullin (1987) in this area to flows with free-stream Mach numbers as high as 0.3. In addition, our results have, for the first time, noted the position of the shock in the recirculating region and the Mach number at which this shock starts to appear.

As noted in §3, the vacuum core boundary treatment currently employed is only approximate, and this treatment causes inaccuracies in results, shown in figure 3. It is hoped that publication of this work will generate new ideas for treatment of this boundary, which could lead to a more complete solution of this flow field.

In spite of problems at the vacuum boundary, the code developed in this study provides a robust scheme for calculating two-dimensional compressible flows by using the solution for the Prandtl–Glauert dipole far from the region in which the vortices are present, and the two-dimensional full potential equation in the region of recirculating flow. A similar procedure could be used to study a compressible line source in a uniform stream, or other basic two-dimensional compressible flow fields.

The authors wish to acknowledge helpful discussions with Professor S. Osher of the Department of Mathematics UCLA. This work has been supported by NASA Ames/Dryden Research Center under Grant NCC 2-374.

Appendix. Application of the Osher flux biasing procedure

The discrete formulae used in the present computations incorporating the flux biasing procedure after Osher *et al.* (1985) and Shankar *et al.* (1987) may be summarized as follows. We begin by defining forward and backward differences in the computational coordinates in the usual way:

$$\phi_{\xi,\mathrm{f}} = (\phi_{i+1,j}-\phi_{i,j})/h, \quad \phi_{\xi,\mathrm{b}} = (\phi_{i,j}-\phi_{i-1,j})/h,$$

where $h \equiv \Delta\xi = \Delta\eta$ is the uniform grid spacing in the computational domain. Analogous formulae hold for the η-derivatives. We then construct the 'clipped' forward and backward approximations to the contravariant velocities as

$$\Phi_{\xi,\mathrm{f}} = \min\left[(x_\eta^2+y_\eta^2)\,\phi_{\xi,\mathrm{f}}-(x_\xi y_\xi+x_\eta y_\eta)\,\phi_{\eta,\mathrm{f}}, 0\right], \tag{A 1}$$

$$\Phi_{\xi,\mathrm{b}} = \max\left[(x_\eta^2+y_\eta^2)\,\phi_{\xi,\mathrm{b}}-(x_\xi y_\xi+x_\eta y_\eta)\,\phi_{\eta,\mathrm{b}}, 0\right], \tag{A 2}$$

etc. The next step is to construct the modified densities of the Osher scheme. As in Shankar *et al.* (1987) we define an intermediate density, $\tilde{\rho}$, based on the streamwise flux biasing formula

$$\tilde{\rho} = \frac{1}{q}\left[\rho q \pm \frac{h}{Q}\left(\Phi_\xi \frac{\partial}{\partial\xi} + \Phi_\eta \frac{\partial}{\partial\eta}\right)(\rho q)^-\right]$$

where

$$Q \equiv (\Phi_\xi^2+\Phi_\eta^2)^{\frac{1}{2}}$$

and

$$(\rho q)^- \equiv \begin{cases} 0 & \text{for} \quad q \leqslant q^* \\ \rho q - \rho^* q^* & \text{for} \quad q > q^*. \end{cases}$$

Here, the asterisk denotes sonic values as given by (2) and (7). Finally, we denote the discretized version of $\tilde{\rho}$ as $F_{l,ij}, l = 1, \ldots, 4$:

$$F_{1,i,j} = \frac{1}{q_{i,j}}\left\{(\rho q)_{i,j} - \frac{1}{Q_{i,j}}\left[\Phi_{\xi,i,j}((\rho q)^-_{i,j}-(\rho q)^-_{i-1,j}) + \Phi_{\eta,i,j}((\rho q)^-_{i,j+1}-(\rho q)^-_{i,j-1})\right]\right\},$$

$$F_{2,i,j} = \frac{1}{q_{i,j}}\left\{(\rho q)_{i,j} + \frac{1}{Q_{i,j}}\left[\Phi_{\xi,i,j}((\rho q)^-_{i+1,j}-(\rho q)^-_{i,j}) + \Phi_{\eta,i,j}((\rho q)^-_{i,j+1}-(\rho q)^-_{i,j-1})\right]\right\},$$

$$F_{3,i,j} = \frac{1}{q_{i,j}}\left\{(\rho q)_{i,j} - \frac{1}{Q_{i,j}}\left[\Phi_{\xi,i,j}((\rho q)^-_{i+1,j}-(\rho q)^-_{i-1,j}) + \Phi_{\eta,i,j}((\rho q)^-_{i,j}-(\rho q)^-_{i,j-1})\right]\right\},$$

$$F_{4,i,j} = \frac{1}{q_{i,j}}\left\{(\rho q)_{i,j} + \frac{1}{Q_{i,j}}\left[\Phi_{\xi,i,j}((\rho q)^-_{i+1,j}-(\rho q)^-_{i-1,j}) + \Phi_{\eta,i,j}((\rho q)^-_{i,j+1}-(\rho q)^-_{i,j})\right]\right\},$$

In these expressions the contravariant velocities are evaluated as the difference between the backward and forward values, (A 1), (A 2).

We note that for $M < 1$ (and hence $q < q^*$), there is no biasing, and the F_l simply reduce to the local density. Furthermore, we remark that the $q_{i,j}$ have been calculated in physical coordinates using first-order upwinding throughout the domain, as is required by Osher's scheme in the supersonic region. In addition, in the region immediately adjacent to the vacuum core (all grid points within three points of the core boundary in the computational domain), the $q_{i,j}$ are smoothed with a low-pass filter often used as a restriction operator in multigrid methods (see Hackbusch 1985) prior to their use in constructing the F_l:

$$q_{i,j} = \tfrac{1}{16}[q_{i-1,j-1} + q_{i-1,j+1} + q_{i+1,j-1} + q_{i+1,j+1} + 2(q_{i-1,j} + q_{i,j-1} + q_{i,j+1} + q_{i+1,j}) + 4q_{i,j}].$$

In Heister (1988) the $\phi_{i,j}$ were filtered, but this has been found to be unnecessary in the present algorithm.

We can now approximate the right-hand side of (21) at each grid point on the interior of the fluid region as

$$\begin{aligned} B_{i,j} = \phi^0_{i,j} - \phi^n_{i,j} + k[&(F_1 \Phi_{\xi,\mathrm{b}})_{i+1,j} - (F_1 \Phi_{\xi,\mathrm{b}})_{i,j} + (F_2 \Phi_{\xi,\mathrm{f}})_{i,j} - (F_2 \Phi_{\xi,\mathrm{f}})_{i-1,j} \\ &+ (F_3 \Phi_{\eta,\mathrm{b}})_{i,j-1} - (F_3 \Phi_{\eta,\mathrm{b}})_{i,j} + (F_4 \Phi_{\eta,\mathrm{f}})_{i,j} - (F_4 \Phi_{\eta,\mathrm{f}})_{i,j-1}]. \end{aligned} \quad \text{(A 3)}$$

REFERENCES

ANDERSON, J. A. 1982 *Modern Compressible Flow with Historical Perspective.* McGraw-Hall.

BROWN, S. N. 1965 The compressible, inviscid leading-edge vortex. *J. Fluid Mech.* **22**, 17–32.

GARABEDIAN, P. 1964 *Partial Differential Equations.* John Wiley.

HACKBUSCH, W. 1985 *Multi-Grid Methods and Applications.* Springer.

HEISTER, S. D. 1988 Transverse jets in compressible crossflows. Ph.D. thesis, University of California, Los Angeles.

KUCHEMAN, D. 1978 *The Aerodynamic Design of Aircraft.* Pergamon.

MACK, L. M. 1959 The compressible viscous, heat-conducting vortex. *Progress Rep.* 20-382. Jet Propulsion Laboratory, Pasadena, CA.

MAXWELL, A. R. 1971 *The Hodograph Equations: An Introduction to The Theory of Plane Transonic Flow.* Hafner.

MOORE, D. W. 1985 The effect of compressibility on the speed of propagation of a vortex ring. *Proc. R. Soc. Lond.* A **397**, 87–97.

MOORE, D. W. & PULLIN, D. I. 1987 The compressible vortex pair. *J. Fluid Mech.* **185**, 171–204.

OSHER, S., HAFEZ, M. & WHITLOW, W. 1985 Entropy condition satisfying approximations for the full potential equations of transonic fluid flow. *Maths Comput.* **44**, 1–29.

RINGLEB, F. 1940 Exakte Losungen der Defferentialgleichungen einer adiabatischen Gasstromung. *Z. Angew. Math. Mech.* **20**, 185–198.

SHANKAR, V., IDE, H., GORSKI, J. & OSHER, S. 1987 A fast, time-accurate, unsteady full potential scheme. *AIAA J.* **25**, 230–238.

SHAPIRO, A. H. 1953 *The Dynamics and Thermodynamics of Compressible Fluid Flow*, Vol. 2. Ronald.

THOMPSON, J. F., WARDI, Z. U. A. & MASTIN, C. W. 1985 *Numerical Grid Generation, Foundations and Applications.* Elsevier/North-Holland.